Development of Classical Potential for $PbTiO_3$

Shi Liu, Hiroyuki Takenaka, Tingting Qi, Ilya Grinberg, and Andrew M. Rappe
The Makineni Theoretical Laboratories, Department of Chemistry,
University of Pennsylvania, Philadelphia, PA, 19104-6323
(Dated: November 26, 2012)

We present a modified bond-valence model of $PbTiO_3$ based on the principles of bond-valence and bond-valence vector conservation. The relationship between bond-valence energy and bond-order potential is derived analytically in the framework of a tight-binding model. A new energy term, bond-valence vector energy, is introduced into the atomistic model and the potential parameters are re-optimized. The new model potential can be applied to both canonical ensemble (NVT) and isobaric-isothermal ensemble (NPT) molecular dynamics (MD) simulations. This model reproduces the experimental phase transition temperature in NVT MD simulations and also exhibits the experimental sequence of temperature-driven and pressure-driven phase transitions in NPT simulations. We expect that this improved bond-valence model can be applied to a broad range of inorganic materials.

The use of ferroelectric perovskite oxides in a variety of technological applications has prompted extensive investigations of their structure and dynamics.[1,2] First-principles density functional theory (DFT) calculations have played an important role in enhancing microscopic understanding of the relationships between composition, structure and properties.[3–5] Despite the success of first-principles methods, the great computational expense and restriction to studying zero-temperature properties have driven the development of more efficient atomistic and effective Hamiltonian potentials suitable for large-scale molecular dynamics (MD) simulations.[6–12]

In particular, an atomistic potential based on the widely used bond-valence (BV) theory[13] was developed by Shin *et al.*[12] BV-based atomistic potentials have since been used to study phase transitions[14] and domain wall motion in $PbTiO_3$[15], as well as structure and dynamics in the classic $0.75PbMg_{1/3}Nb_{2/3}O_3$-$0.25PbTiO_3$ relaxor ferroelectric material.[16] The bond-valence theory, or bond-valence conservation principle, states that in a crystal structure, each atom i prefers to obtain a certain atomic valence, $V_{0,i}$. The actual atomic valence V_i, for atom i can be obtained by summing over the bond valences V_{ij}, which can be calculated from an empirical inverse power-law relationship[17,18] between bond valence and bond length r_{ij}:

$$V_{ij} = \left(\frac{r_{0,ij}}{r_{ij}}\right)^{C_{ij}}. \tag{1}$$

$r_{0,ij}$ and C_{ij} are Brown's empirical parameters. The energy contribution of the bond-valence is chosen to have the following form:

$$E_{BV} = \sum_i S_i (V_i - V_{0,i})^2, \tag{2}$$

where S_i is a scaling parameter.

Despite the success of the rather simple ten-parameter BV model potential[12] for $PbTiO_3$, no rigorous quantum mechanical justification has been provided for the bond-valence potential energy, raising questions about the general applicability of this type of atomistic potential. In addition, the potentials obtained in previous work[12,14] were found to be accurate for NVT simulations only, with incorrect ground state structures obtained when the constant volume constraint is lifted. In this paper, we show how the bond-valence potential can be derived from the second-moment of the local density of states (LDOS), extend the model to represent higher moments and show that this allows accurate simulations for both constant-volume and constant-pressure conditions.

An analysis of the physics that gives rises to the bond-valence conservation principle shows that the bond-valence energy can be naturally derived from the second-moment bond-order potential, such as the well-known Finnis-Sinclair potential.[19,20] Within the framework of a tight-binding model[21], the Finnis-Sinclair potential can be partitioned into atomic contributions as:

$$U_{\mathrm{FS}} = \sum_i \left[\sum_{j \neq i} \phi(r_{ij}) - \gamma_i (\mu_i^{(2)})^{\frac{1}{2}} \right], \tag{3}$$

where $\phi(r_{ij})$ is a pair-wise repulsive potential depending on the distance between atom i and its nearest-neighboring atom j. The second term represents the bonding energy; γ_i is a constant and $\mu_i^{(2)}$ is the second-moment of the LDOS. The second moment $\mu_i^{(2)}$ measures the width of the density of states distribution, and as shown by Cyrot-Lackmann and Ducastelle[22–24] can be evaluated from summation over all the nearest-neighbor hopping paths that start and end on atom i:

$$\mu_i^{(2)} = \sum_{j \neq i} \beta_{ij} \beta_{ji} = \sum_{j \neq i} \beta_{ij}^2, \tag{4}$$

where β_{ij} is the averaged hopping integral between atom i and j. Because the overlap of atomic orbitals decays

as $\exp(-k_{ij}r_{ij})$, Eq.(3) can be written as

$$U_{\rm FS} = \sum_i \sum_{j\neq i} a_{ij} n_i^e n_j^e e^{-2k_{ij}r_{ij}} - \sum_i \gamma_i \left(\sum_{j\neq i} b_{ij} n_i^e n_j^e e^{-2k_{ij}r_{ij}} \right)^{\frac{1}{2}}, \quad (5)$$

where n_i^e is the number of electrons at atom i, a_{ij} is a constant that scales the strength of the repulsive interactions between atom i and atom j, and b_{ij} scales the bonding interaction. The total energy will be minimized when the derivative of $U_{\rm FS}$ with respect to $\exp(-k_{ij}r_{ij})$ is zero. This leads to

$$2a_{ij'} - \frac{\gamma_i b_{ij'}}{\sqrt{\sum_{j\neq i} b_{ij} n_i^e n_j^e e^{-2k_{ij}r_{ij}}}} = 0. \quad (6)$$

After rearranging the terms, we get the minimization condition to be

$$\sum_{j\neq i} b_{ij} n_i^e n_j^e e^{-2k_{ij}r_{ij}} = \frac{\gamma_i^2 b_{ij'}^2}{4a_{ij'}^2}. \quad (7)$$

In the case of a two component system, there is only one type of atomic pair,[25] and therefore b_{ij}/a_{ij} is the same for all the atomic pairs. We can then rigorously define the interatomic bond-valence V_{ij} as

$$V_{ij} \equiv \frac{4V_{0,i} b_{ij} n_i^e n_j^e}{C\gamma_i^2} e^{-2k_{ij}r_{ij}}, \quad (8)$$

where $C = b_{ij}^2/a_{ij}^2$. It is evident that the energy minimization condition becomes

$$V_i = \sum_{j\neq i} V_{ij} = V_{0,i}, \quad (9)$$

which is identical to the bond-valence summation rule. The bond valence of the individual bond V_{ij} corresponds to the hopping integral with $V_{ij} \propto \beta_{ij}^2$. In the case of a more complicated ABO_3 oxide, we would expect that a universal ratio of b_{ij} to a_{ij} for all the cation-anion pairs is still a reasonable assumption.

After substituting Eq.(8) into Eq.(5) and expanding in a Taylor series around $V_{0,i}$, we obtain:

$$U_{\rm FS} = \sum_i \left[-\frac{1}{4} C^{\frac{1}{2}} \gamma_i^2 + \frac{1}{16} \frac{\gamma_i^2 C^{\frac{1}{2}}}{V_{0,i}^2} (V_i - V_{0,i})^2 \right]. \quad (10)$$

Thus, the Finnis-Sinclair energy term (Eq.(3)) and the bond-valence energy (Eq.(2)) are identical for small deviations away from $V_{0,i}$.

Compared to the bond-order potential, the application of the bond-valence model does not require extra efforts to parametrize hopping integrals, because the bond-valence parameters for a wide variety of atomic paris are already known from crystallography.[13] Since the bond-valence model is a second-moment bond-order potential, its limitations, such as the inability to obtain the correct ground state structure in NPT simulations, are likely due to the fact that the second moment only accounts for the width of LDOS but does not reflect its shape. One consequence of this is that the BV energy depends only on the total valence and is entirely insensitive to the number of bonds or their relative strengths. This feature of second-moment models makes it difficult to distinguish between competing crystal structures, which are controlled by the higher moments.[20] Therefore, a systematic way to improve the bond-valence model is to include the contributions of higher moments of the LDOS (such as fourth-moment) to the total energy.[26,27]

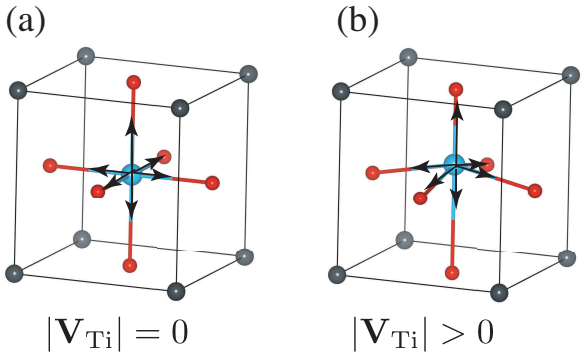

FIG. 1: (Color online) Schematic representation of bond-valence vector summation around Ti in (a) cubic $PbTiO_3$ and (b) tetragonal $PbTiO_3$. Gray, blue and red balls denote Pb, Ti and O. The back arrow scales the magnitude of the bond-valence.

We choose the bond-valence vector sum (BVVS)[13,28] to reflect the change of the fourth moment of the LDOS. The bond-valence vector is defined as a vector lying along the bond with magnitude equal to the bond-valence, as shown in Figure 1. The changes in the local symmetry of the bonding environment that are reflected by the BVVS affect the LDOS shape and the value of the fourth LDOS moment. A simple argument is presented in the Appendix to illustrate the relationship between the fourth moment of the LDOS and the sum of the bond-valence vectors.

For many materials, it has been shown that the ground-state structure favors symmetric local bonding environment and a zero BVVS. Therefore, the criterion of BVVS = 0 for the ground-state structure has been suggested as a complement to the original bond-valence conservation principle.[13,28] However, this is not true for crystal structures in which symmetry breaking (BVVS $\neq$ 0) becomes significant due to electronic-

structure driven distortions, such as the second order Jahn-Teller distortion exhibited by Ti atoms in an octahedral environment and the stereochemical long-pair driven distortion present in $Pb^{2+}$and Bi^{3+} cations. The BVVS can thus be considered as a measure of local symmetry breaking. We therefore generalize this principle by proposing that each ion has a desired length of bond-valence vector summation. The bond-valence vector energy, E_{BVV}, is defined as

$$E_{BVV} = \sum_i D_i (\mathbf{V}_i^2 - \mathbf{V}_{0,i}^2)^2 \quad (11)$$

where D_i is the scaling factor, $\mathbf{V}_i$ is the calculated bond-valence vector summation and $\mathbf{V}_{0,i}$ is the desired value of bond-valence vector summation. The value of $\mathbf{V}_{0,i}$ can be computed using the optimized atomic positions in the lowest-energy structure from first-principles.

The interatomic potential for our modified bond-valence model is given by:

$$E = E_c + E_r + E_{BV} + E_{BVV} + E_a \quad (12)$$

$$E_c = \sum_{i<j} \frac{q_i q_j}{r_{ij}} \quad (13)$$

$$E_r = \sum_{i<j} \left(\frac{B_{ij}}{r_{ij}} \right)^{12} \quad (14)$$

$$E_a = k \sum_i^{N_{\rm oct}} (\theta_{i,x}^2 + \theta_{i,y}^2 + \theta_{i,z}^2) \quad (15)$$

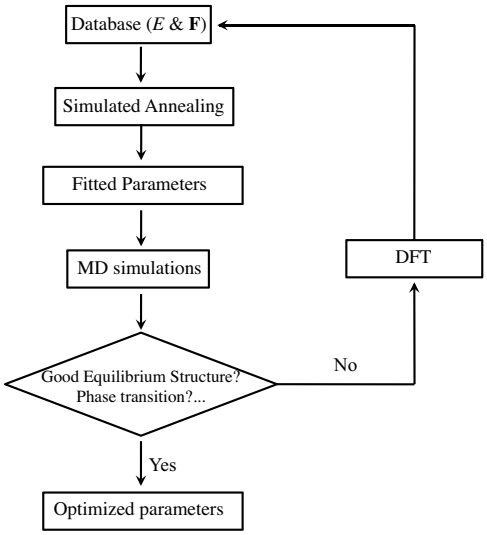

FIG. 2: Potential optimization protocol used in this work.

TABLE I: Optimized potential parameters of modified bond-valence model. Then angle potential parameter k is 3.14 meV/(deg)^2

				$B_{\beta\beta'}$(Å)				
	q_β(e)	S_β(eV)	D_β	Pb	Ti	O	$V_{0,\beta}$	$\mathbf{V}_{0,\beta}$
Pb	1.38177	0.31646	2.23180	–	2.06058	1.70871	2.00	0.40297
Ti	0.99997	–	0.11888	–	–	1.29532	4.00	0.46541
O	-0.79391	1.52613	–	–	–	1.88109	2.00	–

where E_c is the Coulomb energy, E_r is the short-range repulsive Lennard-Jones energy. It is noted that all the atomic orbitals are approximated as s-type and only averaged hopping integrals between neighboring atoms are used in both Finnis-Sinclair potential and the BV energy. However, bonding in $PbTiO_3$ involves p and d orbital overlaps, which do display angular dependence. To introduce the dependence of energy on the interatomic angles, we used an angle potential, E_a, which prevents unphysically large tilting of oxygen octahedra. The potential parameters required from fitting can be summarized as follows: spring constant k, charges q_i, scaling factors S_i and D_i for each species and short-range repulsion parameters, B_{ij}, for all the pairs of Pb-Ti, Pb-O, Ti-O and O-O. Due to the charge-neutrality constraint, there are thirteen independent parameters.

Figure 2 shows our parameterization protocol. The optimization of the potential parameters is performed using simulated annealing (SA) global optimization method to fit a database of structural energy differences and atomic forces (E & $\mathbf{F}$) derived from *ab initio* DFT calculations with the *Abinit* code.[29] We used the $2\times2\times2$ supercell as the reference structure. The energy and atomic forces are computed with $2 \times 2 \times 2$ Monkhorst-Pack k-point mesh[30] using PBEsol [31] as the exchange-correlation energy functional. We start with an ini-

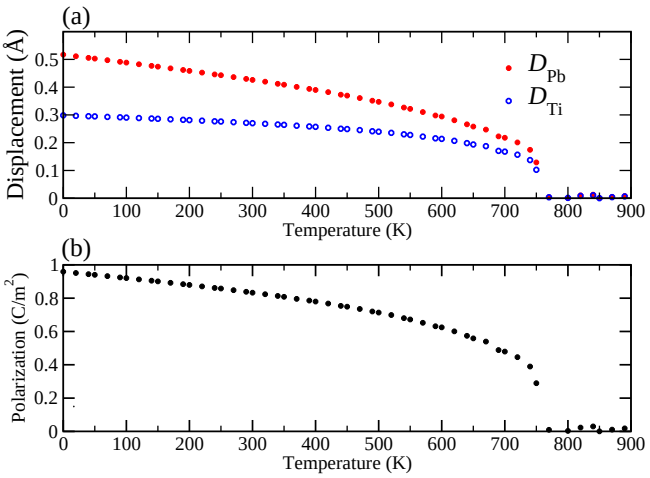

FIG. 3: (Color online) Temperature dependence of (a) atomic displacements of Pb and Ti, and (b) spontaneous polarization obtained from NVT MD simulations with lattice constants fixed to experimental values.

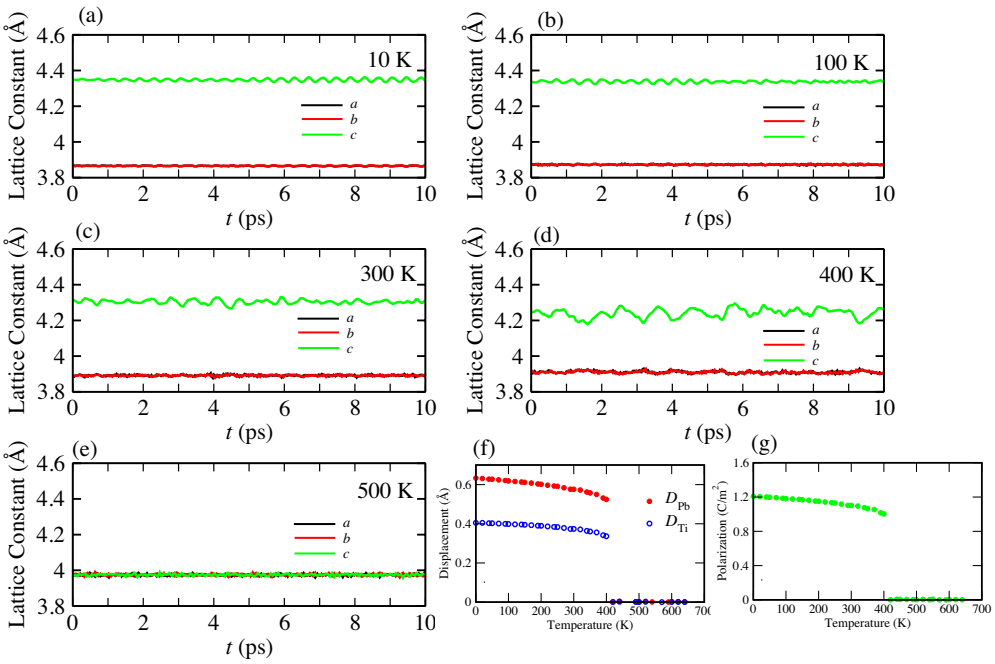

FIG. 4: (Color online) Temperature-dependent properties of $PbTiO_3$ obtained from NPT simulations. (a)-(e) Profiles of lattice constants from MD simulation. (f) Atomic displacements of Pb and Ti as a function of temperature. (g) Spontaneous polarization as a function of temperature.

tial database that contains the lowest-energy tetragonal structure, strained tetragonal structures, the lowest-energy cubic structure, strained cubic structures, and randomly picked orthorhombic structures with various lattice constants. After each SA run, the optimized potential parameters are used to perform constant-stress MD simulations to generate equilibrium structures at various temperatures, which are then put back to the database. The process is continued until the energies of the structures sampled during MD simulations accurately reproduced and the simulation therefore reproduces the DFT ground state and correct phase transition behavior.

Table I presents the optimized potential parameters. To account for the overestimation of the $PbTiO_3$ c/a ratio by PBEsol (c/a=1.10 versus c/a=1.07 experimentally)[32], we adjusted Brown's empirical parameter r_{ij}^0 to make the V_β for Pb, Ti and O reach their atomic valences in the lowest-energy tetragonal structure. The value of preferred vector summation is then calculated with the modified empirical parameters. We found that the oxygen atoms do not have a preference for a specific value of bond-valence vector sum. This is because in perovskites, some oxygen atoms are highly displaced ($|\mathbf{V}_O| > 0$), while others stay around the high-symmetry point ($|\mathbf{V}_O| = 0$). Therefore, we set the scaling factor D_O for oxygen atoms to be zero. During the parameter fitting, we also consistently found that the optimized scaling factor S_{Ti} is zero, which implies that for $PbTiO_3$ only two scaling factors of the bond-valence energy are independent, due to the bond-valence conservation principle.

Using this optimized model potential, we studied the temperature dependence of lattice constants, polarization and displacements of Pb and Ti using an $8 \times 8 \times 8$ supercell. We first performed canonical-ensemble MD simulation with lattice constants fixed to experimental values, using the Nosé-Hoover thermostat to control the temperatures. For these simulations, we obtained 760 K for the ferroelectric-to-paraelectric first-order phase transition temperature T_c, shown in Figure 3. This agrees well with the experimental T_c of 765 K and is an improvement relative to the 550 K values obtained by the NVT calculations with the original BV potential.[12,14] We then used the new potential in NPT simulations, with the pressure maintained at 0.1 MPa by the Parrinello-Rahman barostat. For the ground state structure at 0 K, we obtained the lattice constant a=3.865 Å and c/a=1.12. The c/a ratio in MD is slightly larger than the PBEsol DFT value. Figure 4 displays the temperature dependence of lattice constants, spontaneous polarization and atomic displacements of Pb and Ti obtained from NPT simulations. As temperature increases, the c/a ratio decreases gradually, together with the polarization and atomic displacements. The phase transition from tetragonal to cubic occurs at 400 K, lower than the experimental value. The rather large magnitude of spontaneous polarization and the atomic displacements at temperatures just below T_c are due to the overestimated tetragonality of the PBEsol functional and the resulting potential.

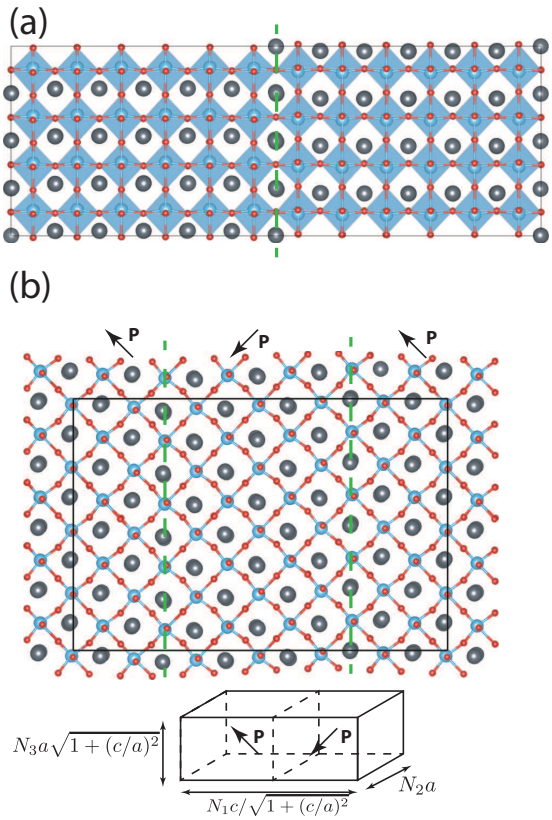

FIG. 5: (Color online) Simulated domain wall using modified bond-valence model. (a) 180° domain wall constructed with a 12×4×4 supercell; (b) 90° domain wall with $N_1 = 12$, $N_2 = 4$, $N_3 = 4$.

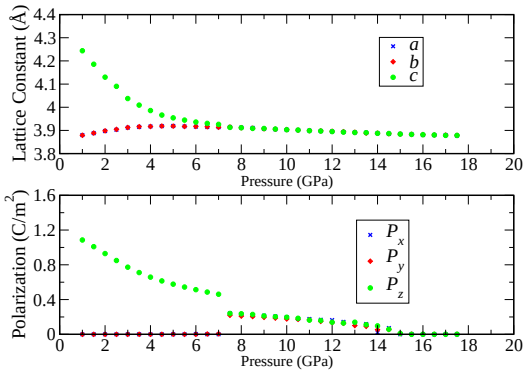

FIG. 6: (Color online) Pressure-induced phase transitions of $PbTiO_3$ obtained from MD simulations. Lattice axes coincide with the Cartesian axes (a along x, b along y and c along z).

We find that the new potential is capable of describing the domain wall (DW) energetics and structure. The supercell used to model the domain wall is constructed following the method in Ref. 32. The domain wall energy ($E_{\rm DW}$) is calculated by

$$E_{\rm DW} = \frac{E_N - E_{\rm bulk}}{S_{\rm DW}}, \qquad (16)$$

where E_N is the energy of the supercell, $E_{\rm bulk}$ is the energy of a single-domain supercell of the same size, and $S_{\rm DW}$ is the area of the domain wall. Figure 5(a) presents simulation of 180° Pb-centered domain walls at 10 K. The computed domain wall energy is 161 mJ/m^2 and agrees very well with 170 mJ/m^2 obtained via PBEsol DFT calculations (with a $8 \times 1 \times 1$ supercell). To simulate a 90° domain wall, we used a supercell with $N_1 = 12$, $N_2 = 4$, and $N_3 = 4$, as shown in Figure 5(b). The dimensions of the supercell are fixed to the values calculated based on experimental lattice constants of tetragonal $PbTiO_3$. The domain wall energy is estimated to be 70 mJ/m^2 and also shows a satisfying agreement with the PBEsol DFT value of 64 mJ/m^2 (with a $8 \times 1 \times 1$ supercell). We note that the BV potential is highly efficient, as all the interactions are pair-wise and only depend on distance. This allows simulations of 30×30×4 supercell (18000 atoms) for 15 ps with a 0.3 fs timestep using only 33678 seconds of CPU time (10 minutes of wall clocktime parallelized over 48 CPUs on the Cray XT5 supercomputer at the Navy DoD Supercomputing Resource Center).

We have also examined the performance of the potential in simulations of pressure-induced phase transitions in $PbTiO_3$ with a $10 \times 10 \times 10$ supercell. Figure 6 shows the pressure dependence of lattice constants and polarization. We found two phase transitions, at 7 GPa and 15 GPa. Below 7 GPa, the structure is ferroelectric. The tetragonality decreases with increased pressure and the magnitude of polarization along the long axis reduces accordingly. Above 7 GPa, the c/a ratio becomes 1 but the structure maintains ferroelectricity up to 15 GPa. The polarization is mostly along [111] direction between 7 GPa and 15 GPa, suggesting the existence of rhombohedral phase. The polarization disappears when the pressure exceeds 15 GPa and the structure becomes the centrosymmetric paraelectric. Our simulated results are consistent with Wu and Cohen's first-principles studies[34,35] and recent experimental results by Ahart *et al.*[36] We did not find any reentrance of ferroelectricity up to 60 GPa.

We improved our bond-valence model by introducing a new energy term, bond-valence vector energy, based on an extension of the bond-valence vector conservation principle. This new 12-parameter potential reproduces the polarization, ferroelectric instability and phase transition temperature in NVT simulations, and also captures the temperature-driven phase transition qualitatively in NPT simulations. Both calculated 180° DW energy and 90° DW energy using this new potential are in good agreement with DFT values. This new potential is efficient enough to simulate large domain walls. The studies of pressure-induced phase transition

with the new potential show two phase transitions, consistent with previous experimental studies. We hope that this improved bond-valence model will also be applied to other oxides due to its simplicity, efficiency and accuracy.

S.L. was supported by the NSF through Grant CBET-0932786. H.T. was supported by the US DOE BES under Grant No. DE-FG02-07ER46431. I.G. was supported by the Energy Commercialization Institute. T.Q. and A.M.R. were supported by the US ONR under Grant No. N00014-11-1-0578. Computational support was provided by the Center for Piezoelectrics by Design, and by the DoD HPCMO.

APPENDIX

The bond valence of an individual bond V_{ij} has been shown to be proportional to the square of hopping integral β_{ij}. Both the bond-valence vector sum, $\mathbf{V}_i$, and the fourth-moment of the LDOS, $\mu_i^{(4)}$, can reflect the change of local symmetry of bonding environment. Figure A1 gives an example of a one-dimensional AB alloy. The desired bond valence of $A-B$ in the undistorted structure is set to be a, and therefore the hopping integral is equal to $\sqrt{\gamma a}$, where γ is a constant. It is easy to calculate that the bond valence summation and $\mu^{(2)}$ at atom A are $2a$ and $2\gamma a$, respectively. The small displacement in the distorted lattice changes the bond-valence of the longer $A-B$ bond to $(a-\delta)$ and the shorter one to $(a+\delta)$. Accordingly, the hopping integral for the longer $A-B$ is $\sqrt{\gamma(a-\delta)}$ and the shorter one $\sqrt{\gamma(a+\delta)}$. The bond-valence conservation principle holds in both structures. However, the $\mathbf{V}_A$ changes from zero in the undistorted structure to 2δ in the distorted structure, and the $\mu_A^{(4)}$ is reduced from $6\gamma^2a^2$ to $6\gamma^2a^2-2\gamma^2\delta^2$. It is evident that only the hopping path involving the next-nearest neighbors contributes to the change of fourth-moment. Therefore, the change of fourth moment, $\Delta\mu_i^{(4)}$, can be approximated with $(|\mathbf{V}_i|-|\mathbf{V}_{i,0}|)^2$. We choose $\mathbf{V}_i^2$ instead of $|\mathbf{V}_i|$ in the formula of E_{BVV} to make sure E_{BVV} is a differentiable function for each $\mathbf{V}_i$.

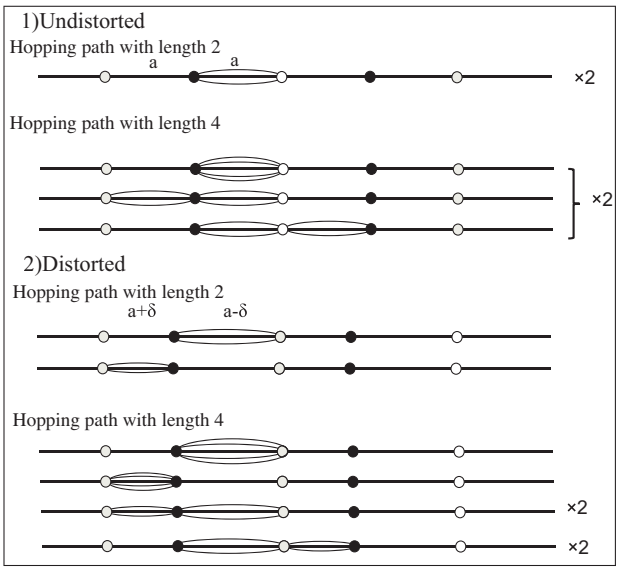

FIG. A1: Hopping integrals in one-dimensional AB alloy. Empty and filled circles represent elements A and B.

[1] M. E. Lines and A. M. Glass, *Principles and Applications of Ferroelectrics and Related Materials* (Clarendon Press, Oxford, 1977).
[2] J. F. Scott, Science **315**, 954 (2007).
[3] R. E. Cohen, Nature **358**, 136 (1992).
[4] W. Zhong, R. D. King-Smith, and D. Vanderbilt, Phys Rev Lett **72**, 3618 (1994).
[5] I. Grinberg and A. M. Rappe, Phys Rev B **70**, 220101 (2004).
[6] M. Sepliarsky and R. E. Cohen, AIP Conf. Proc. **626**, 36 (2002).
[7] T. Shimada, K. Wakahara, Y. Umeno, and T. Kitamura, J. Phys.: Condens. Matter, **20**, 325225 (2008).
[8] M. Sepliarsky, A. Asthagiri, S. R. Phillpot, M. G. Stachiotti, and R. L. Migoni, Curr. Opin. Solid State Mater. Sci. **9**, 107 (2005).
[9] I. Grinberg, V. R. Cooper and A. M. Rappe, Nature **419**, 909 (2002).
[10] W. Zhong, D. Vanderbilt, and K. M. Rabe, Phys. Rev. B **52**, 6301 (1995).
[11] U. V. Waghmare and K. M. Rabe, Phys. Rev. B **55**, 6161 (1997).
[12] Y.-H. Shin, V. R. Cooper, I. Grinberg and A. M. Rappe, Phys. Rev. B **71**, 054104 (2005).
[13] I. D. Brown, Chem. Rev. **109**, 6858 (2009).
[14] Y.-H. Shin, J.-Y. Son, B.-J. Lee, I. Grinberg, and A. M. Rappe, J. Phys.: Cond. Matt. **20**, 0152241 (2008).
[15] Y.-H. Shin, I. Grinberg, I.-W. Chen and A. M. Rappe,Nature **449**, 881 (2007).
[16] I. Grinberg, Y.-H. Shin, and A. M. Rappe, Phys. Rev. Lett. **103**, 197601 (2009).
[17] I. Brown and R. Shannon, Acta Cryst. A **29**, 266 (1973).
[18] I. Brown and K. K. Wu, Acta. Cryst. B **32**, 1957 (1976).
[19] M. W. Finnis and J. E. Sinclair, Philos. Mag. A, **50**, 45 (1984).
[20] A. P. Sutton, *Electronic structure of materials* (Oxford University Press, 2004).
[21] A. P. Horsfield, A. M. Bratkovsky, M. Fearn, D. G. Pettifor, and M. Aoki, Phys. Rev. B **53**, 12694 (1996).
[22] F. Cyrot-Lackmann, J Phys. Chem. Solids **29**, 1235 (1968).
[23] F. Cyrot-Lackmann, Phys. Rev. B **29**, 2744 (1980).
[24] F. Ducastelle and F. Cyrot-Lackmann, J. Phys. Chem. Solids **32**, 285 (1971).
[25] Bond-valence model is expressed entirely in terms of nearest neighbor interactions. The bond is defined between atoms of different electronegativity. Therefore, in a two-component system, AB, there is only one type of bond, A-B, as A and B have different electronegativity. The A-A and B-B interactions are not considered in bond-valence model.
[26] A. E. Carlsson, and N. W. Ashcroft, Phys. Rev. B **27**, 2101 (1983).
[27] L. Hansen, P. Stoltze, K. W. Jacobsen, and J. K. Nørskov, Phys. Rev. B **44**, 6523 (1991).
[28] M. A. Harvey, S. Baggio, and R. Baggio, Acta Crystallogr. **B62**, 1038, (2006).
[29] X. Gonze *et al.*, Comp. Mater. Sci. **25**, 478 (2002).
[30] H. J. Monkhorst and J. D. Pack, Phys. Rev. B **13**, 5188 (1976).
[31] J. P. Perdew *et al.*, Phys. Rev. Lett. **100**, 136406 (2008).
[32] Y. Zhao and D. G. Truhlar, J. Chem. Phys. **128**, 184109 (2008).
[33] B. Meyer and D. Vanderbilt, Phys Rev B **65**, 104111 (2002).
[34] Z. Wu and R. E. Cohen, Phys. Rev. Lett.**95**, 037601 (2005).
[35] P. Ganesh and R. E. Cohen, J. Phys.: Condens. Matter, **21**, 064225 (2009).
[36] M. Ahart *et al.*, Nature (London) **451**, 545 (2008).